Journal of Balkan Science and Technology

journal homepage: www.jbst.nku.edu.tr/

Comparison of phase calculation methods for quantitative phase imaging

Özlem KOCAHAN[1], Erhan TİRYAKİ[2*]

[1]Department of Physics, Faculty of Arts and Sciences, Tekirdağ Namik Kemal University, 59030, Tekirdag, Turkey
[2]Marelli Mako Turkey Elektric San. Tic. A.Ş., 16140, Bursa, Turkey

ABSTRACT

A comparison of different phase calculation methods that can be used to obtain phase information from the fringes formed by diffraction phase microscopy is presented. As a quantitative phase imaging method, white light diffraction phase microscopy can provide an interferogram non-invasively. Thin film surface interferograms have been retrieved by the white light diffraction phase microscopy which is composed of an optical microscope and a Mach–Zehnder interferometer. There are several techniques for the determination of phase from interferograms. Fourier transform and continuous wavelet transform are the most commonly used methods for phase calculation. Stockwell transform is defined as a phase-corrected version of the continuous wavelet transform method, which is the basis of multi-resolution signal analysis methods. In this study, for the phase calculation of interferograms, Fourier transform, continuous wavelet transforms with Morlet, Paul and zero-order generalized Morse wavelet, and Stockwell transform phase methods have been compared in terms of the precision and the implementation.

1. Introduction

Although electron microscopy or atomic force microscopy offers a high spatial resolution, optical microscopy, having the advantages of being non-invasive, high accuracy and speed, has been a backbone for biomedical research [1]. Optical 3-D profilometry has been mostly preferred for live-cell imaging, industry monitoring, etc. because of these advantages [2]–[5]. Interferometry is one of the most useful tools which provides quantitative phase information about the surface morphology [6].

There are several options for quantitative phase imaging, which can be best classified as phase-shifting, common-path, white light, and off-axis interferometry. As a quantitative phase imaging technique, diffraction phase microscopy (DPM) has a quasi-common-path configuration and uses a Mach-Zehnder interferometer including a camera, a pinhole filter, 4f lens system, a grating [7]. This setup with white light allows low noise and single-shot measurement [8]–[10]. Also, it is non-destructive, since the sample with interference fringes can be obtained from DPM without coating or painting [10]–[13]. DPM combines the advantages of off-axis holography-specific velocity and phase sensitivity associated with common-path interferometry [7], [14], [15].

Fourier transform (FT) is the most commonly used time-frequency analysis for the phase calculation from an interferogram formed by quantitative phase imaging setups [16]–[19]. If the existing spectral components in the signal would be needed, the FT can handle it. However, the Fourier transform is not useful if the time interval of the component is also needed [20], [21].

One of the popular phase calculation techniques used successfully in the analysis of fringe patterns is the continuous wavelet transform (CWT), which can provide frequency and time information simultaneously using different wavelets [22]–[25]. The most significant property of the CWT is that for every single spectral component the wavelet function is changing. Because of this property, CWT can better solve the local characteristics and increase the measurement accuracy. The Morlet wavelet is controlled by a fixed spatial frequency of 5 or 6 to satisfy the admissibility condition [18], [24], [26]. Paul wavelet can change the resolution by the variable parameter [27]. Generalized morse wavelets (GMW) have been defined as eigenfunctions of a time-frequency localization operator, which have the advantage of two degrees of freedom [28], [29]. The extra degrees of freedom leads to control of the precision of the measurement.

Stockwell transform (ST) is another time-frequency analysis method which has a frequency-dependent Gaussian window localizing the complex Fourier sinusoid [30]–[33]. According to the definition of ST, while the window function localizes and shifts in time-space, the exponential kernel (Fourier sinusoid function) remains unchanged. In this way, the real and imaginary components are localized independently in the S-Transform. As well as the phase spectrum it localizes the amplitude spectrum. This is called absolute reference phase information [34]–[36].

* Corresponding author: Tekirdağ Namık Kemal University, Faculty of Arts and Sciences, Department of Physics, Kampüs Cd. No:1, 59030 Tekirdağ/TURKEY
E-mail: okocahan@nku.edu.tr

In this study, to acquire an interferogram of a thin film surface, the white light DPM has been chosen because of the single-shot measurement and low noise properties. The phase values have been calculated from these images by using FT, CWT, and ST. Thus, it is possible to see the differences in sensitivity and application among the most used methods in phase calculation.

2. FT Method

The phase term carries the height information of the interferogram; hence, the surface profile can be obtained by calculating the phase value for each point of the interferogram image. FT is a commonly used method of phase demodulation from an interferogram. In the FT method, discrete fast FT is applied to obtain the spectrum of the interferogram, and the fundamental spectrum is subtracted, then the inverse FT is applied. Therefore, the wrapped phase is retrieved and unwrapped for the phase information of the sample [16], [37], [38]. When the Fourier transform of the signal defined in the time domain is taken, it is obtained how much of each frequency is found. However, the processed signal has no information on what timerange these frequency components are located.

3. CWT Method

CWT is used in the time-frequency representation of time series. The time and frequency resolution problem are related to the Heisenberg Uncertainty Principle of quantum mechanics. In CWT, the signal is multiplied with a function similar to the window function, and the window width changes as each spectral component is processed, this is the most basic feature of the CWT [26]. The mathematical expression of CWT is given as [39]

$$CWT(a,b) = \int_{-\infty}^{\infty} h(x)\psi_{a,b}^*(x)\, dx \tag{1}$$

Here, b is the translation parameter, a is the scale parameter and $h(x)$ is a 1D fringe signal, $\psi_{a,b}^*(x)$ is the complex conjugate of the analyzing wavelet function. CWT can be expressed in terms of FT as

$$CWT(a,b) = \sqrt{a} \int_{-\infty}^{+\infty} \hat{\psi}_{a,b}^*(a\alpha)\hat{H}(\alpha)\, exp(ib\alpha)d\alpha. \tag{2}$$

$\hat{\psi}_{a,b}^*(\alpha)$ and $\hat{H}(\alpha)$ are the FT of $h(x)$ and $\psi_{a,b}^*(x)$ in α domain [24]. The selection of a mother wavelet is a point that needs attention according to the application to be made. In this study, Morlet, GMW, and Paul wavelet were used to phase calculation. The Morlet wavelet is defined as

$$m(x) = \pi^{1/4} exp(icx) exp(-x^2/2) \tag{3}$$

and its Fourier transform as

$$\hat{M}(\alpha) = \frac{\sqrt{2\pi}}{\sqrt[4]{\pi}} exp\left[-\frac{(\alpha-c)^2}{2}\right] \tag{4}$$

where c is a fixed spatial frequency [26]. The n order Paul wavelet is formulated by [27]

$$p(x) = \frac{2^n n!\,(1-ix)^{-(n+1)}}{2\pi\sqrt{(2n)!/2}} \tag{5}$$

Its FT is

$$\hat{P}(\alpha) = \frac{2^n}{\sqrt{n(2n-1)!}}\alpha^n exp(-\alpha)\Im(\alpha) \tag{6}$$

where $\Im$ is the Heaviside distribution [40].

Zero order GMW has been defined in the α domain [41].

$$\widehat{GM}_{\beta,\gamma}(\alpha) = \Im(\alpha)\kappa_{\beta,\gamma}\alpha^\beta exp(-\alpha^\gamma) \tag{7}$$

where $\kappa_{\beta,\gamma} \equiv 2(e\gamma/\beta)^{\beta/\gamma}$ normalization coefficient and e is Euler number. β and γ are the variable parameters which lead to precision in the calculation of phase [42].

Morlet wavelet has the minimum uncertainty $\Delta x \times \Delta\alpha = 1/2$ [24] and the Paul wavelet produces uncertainty as $\Delta x \times \Delta\alpha = 1/2\sqrt{(2n+1)/(2n-1)}$ [27], [40]. Thus, Paul provides a better localization than the Morlet wavelet due to its variable parameter n. GMWs provide a good alternative due to having two variable parameters. For different GMWs' parameters, uncertainties were analyzed by Kocahan et al. [42]. Uncertainties for GMW, Morlet, Paul wavelets and ST are compared in table 1. Since FT works like an infinite window function, it has no uncertainty value.

Table 1. Uncertainties for some β and γ values of GMW, Morlet, Paul, and ST

			β		
		3	5	7	10
GMW	γ	3			
		0.50	0.50	0.50	0.50
		5			
		0.51	0.51	0.51	0.50
		7			
		0.53	0.52	0.52	0.51
		10			
		0.57	0.55	0.54	0.53
Paul	n	1	2	10	20	50
		0.86	0.64	0.52	0.51	0.50
Morlet	0.50				
ST	0.50				

The 1D fringe signal [24]

$$h(x) = I_0(x)[1 + V(x)\cos(2\pi f_0 x + \varphi(x))] \qquad (8)$$

where f_0 is the spatial carrier frequency, $\varphi(x)$ is the phase of the fringe, $V(x)$ is the visibility and $I_0(x)$ is the intensity of the background. In order to recover the phase, f_0 must satisfy

$2\pi f_0 \rangle \left| \frac{d\varphi}{dx} \right|_{max}$ condition [1]. Within consideration that $\hat{H}(a\alpha) = 0$ for $\alpha \leq 0$, substituting FT of the fringe signal $\hat{H}(\alpha)$ and Morlet wavelet $\hat{M}(\alpha)$ into equation (2), CWT with Morlet wavelet is obtained as equation (9). Similar to the Morlet wavelet, to introduce the Paul wavelet transform, FT of the fringe signal $\hat{H}(\alpha)$ and Paul wavelet $\hat{P}(\alpha)$ are substituted into equation (2), and it becomes as equation (10).

$$CWT_M(b,a) = I_0(b)V(b)\pi^{5/4}\sqrt{2a}\,exp\left\{\frac{[a(2\pi f_0 + \varphi'(b)) - c^2]}{2}\right\}exp\{i[\varphi(b) + 2\pi f_0 b]\} \qquad (9)$$

$$CWT_P(b,a) = \frac{I_0(b)V(b)a^{n+1/2}[2\pi f_0 + \varphi'(b)]^n\,exp\{[-a(2\pi f_0 + \varphi'(b))]\}}{(2n)!}exp\{i[\varphi(b) + 2\pi f_0 b]\} \qquad (10)$$

Finally, CWT for the zero-order GMW is retrieved as

$$CWT_{GMW}(a,b) = 2\pi I_0(b)V(b)\left(\frac{\gamma}{\beta}\right)^{\beta/\gamma}\exp\left(\frac{\beta}{\gamma}\right)a^{\beta+\frac{1}{2}}$$
$$\times\left[\left(f_0 + \frac{\varphi'}{2\pi}\right)^\beta\exp\left(-\left(af_0 + a\frac{\varphi'}{2\pi}\right)^\gamma\right)\right]\left[\exp\left(i\left(\varphi(b) - b\varphi'(b) + bf_0 + b\frac{\varphi'}{2\pi}\right)\right)\right] \qquad (11)$$

From this CWT equation, wrapped phase values can be calculated by $\varphi(b) = tan^{-1}\left(\frac{ImCWT}{ReCWT}\right)$. By unwrapping the wrapped phase $\varphi(b)$, the correct phase distribution is acquired.

4. ST Method

The ST includes an exponential kernel multiplied by a Gaussian window. ST of the fringe signal is given as [34]

$$ST(b,f) = \int_{-\infty}^{\infty} h(x)\,w(b - x,f)\exp(-i2\pi f x)dx, \qquad (12)$$

where $w(b - x, f)$ is the generalized Gaussian window

$$w(b - x,f) = \frac{|f|}{\sqrt{2\pi}}exp\left(-\frac{f^2(b-x)^2}{2}\right) \qquad (13)$$

with frequency f, parameter b controlling the position of the Gaussian window on the x-axis. The Gaussian window in the Fourier domain is

$$\hat{W}(\alpha,f) = \exp\left(-\frac{2\pi^2\alpha^2}{f^2}\right). \qquad (14)$$

ST can be defined in Fourier domain with Fourier transform of the fringe signal $\hat{H}(\alpha)$ and Gaussian window $\hat{W}(\alpha,f)$ [34]

$$ST(b,f) = \int_{-\infty}^{\infty} \hat{W}(\alpha,f)\,\hat{H}(\alpha + f)\exp(i2\pi b\alpha)d\alpha. \qquad (15)$$

The Gaussian window provides minimum uncertainty $\Delta x \times \Delta \alpha = 1/2$. Inserting Fourier transform of the fringe signal $\hat{H}(\alpha)$ and Gaussian window $\hat{W}(\alpha,f)$, and noting that $\hat{W}(\alpha,f) = 0$ for $\alpha \leq -f$, ST is obtained as

$$ST(b,f)7 = \pi I_0 V exp\left\{-\frac{2\pi^2}{f^2}\left[-f + f_0\right.\right.$$
$$\left.\left. + \frac{\varphi'}{2\pi}\right]^2\right\}exp\{i[\varphi + 2\pi bf_0 \qquad (16)$$
$$- 2\pi bf]\}.$$

The wrapped phase values can be calculated by $\varphi(b) = tan^{-1}\left(\frac{ImST}{ReST}\right)$. By unwrapping the wrapped phase $\varphi(b)$, the correct phase distribution is acquired.

5. Results and Discussion

5.1 Simulation Study

Above mentioned phase methods were tested with the phase function $\varphi(x,y) = [peaks(300)]$ (Fig. 1). The interferogram with this phase function was acquired by using $f_0 = 0.37$ (1/pixel), $V(x) = 1.0$ and $I_0(x) = 1.0$ in the fringe signal as indicated in Fig. 2. By using FT, CWT with Morlet, Paul, GMW and ST, phases were calculated for each pixel and the obtained wrapped phases were unwrapped to correct the phase discontinuities. The absolute phase errors were determined as the difference between the calculated and test phases and plotted in Fig. 3. In table 2, the phase errors for four different pixel numbers were given, which were calculated from the difference between the simulated and calculated phases.

In CWT, Paul wavelet and GMW can control the precision by the variable parameters which lead to a change in uncertainty value as can be seen in table 1. The simulation study, carried out with FT, CWT with Morlet, Paul, and GMW as well as ST, discloses that the results are compatible with the

test phase as shown in Fig. 3. The simulations reveal minimum absolute phase error to be retrieved for CWT with Paul wavelet and GMW as in this Figure and table 2. CWT with Paul wavelet and GMW give % 0.0405 and %0.0238 mean phase errors respectively which are the best error values in table 2.

According to Tables 1 and 2, an extra degree of freedom improves the flexibility of uncertainty value and measurement accuracy; Paul wavelet and GMW have this advantage with variable parameters.
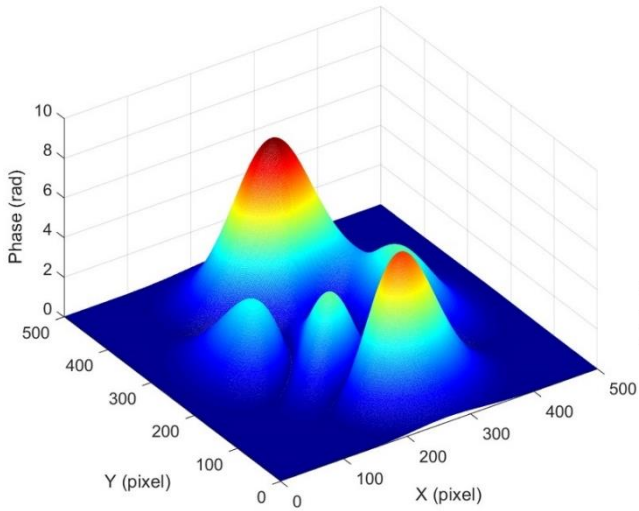
Fig. 1 Simulated phase.
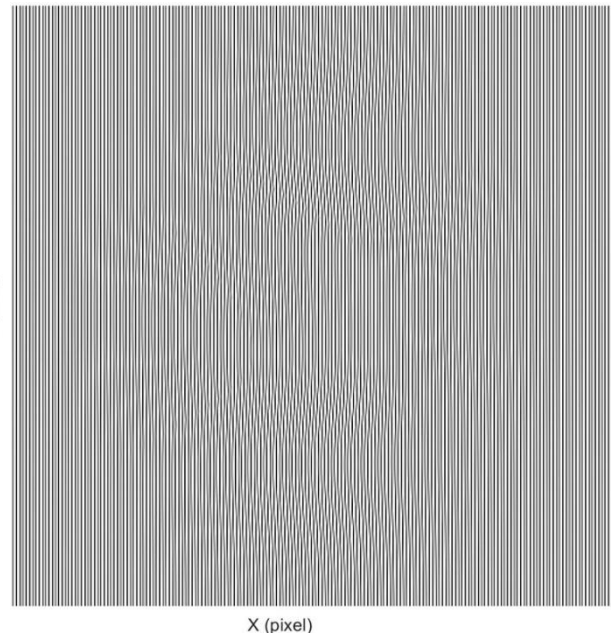
Fig. 2 Simulated fringe pattern with the phase.
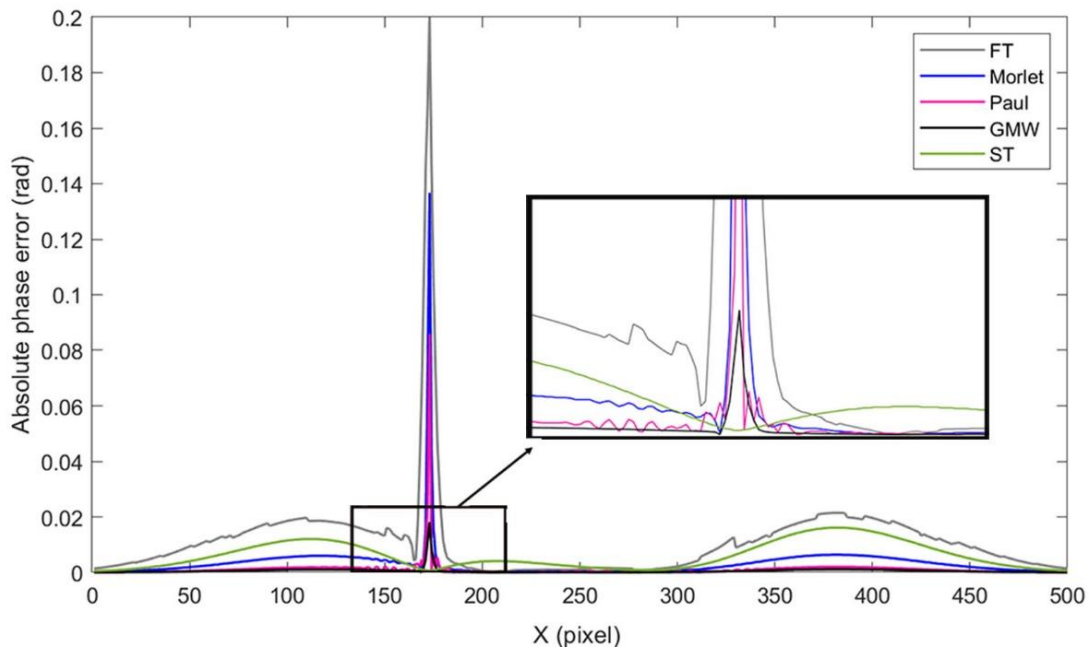
Fig. 3 The absolute phase error was calculated for the line x=250 by FT, CWT with Morlet, Paul (n=10), GMW (β=10; γ=3) and ST.

Table 2. Comparison of phase values in radiant and phase errors for four different pixel numbers

Pixel number	250x50	250x150	250x250	250x350
Phase values				
FT	2.0026	3.0751	1.0161	5.8261
CWT-Morlet	2.0195	3.0969	1.0179	5.8506
CWT-Paul (n=10)	2.0209	3.0992	1.0179	5.8539
CWT-GMW (β=10; γ=3)	2.0211	3.1007	1.0179	5.8544
ST	2.0188	3.0956	1.0179	5.8488
Simulated phase	2.0214	3.1015	1.0183	5.8553
Phase error (%)				
FT	0,9300	0,8512	0,2160	0,4987
CWT-Morlet	0,0940	0,1483	0,0393	0,0803
CWT-Paul (n=10)	0,0247	0,0742	0,0393	0,0239
CWT-GMW (β=10; γ=3)	0,0148	0,0258	0,0393	0,0154
ST	0,1286	0,1902	0,0393	0,1110

5.2 Experimental work

An interferogram image of the sample is needed to calculate the phase distribution and to determine the 3D profile of the surface. CdS thin film was used as a sample in this work. To obtain an interferogram, we used DPM setup (Fig. 4) which uses a Mach–Zehnder interferometer and an optical microscope with a halogen lamp [23]. Axio Observer A1 Zeiss Inverted microscope and 40X objective were used for the observation of the thin film surface. Amplitude grating (110 grooves per mm), located in front of the image output of the microscope, is the first component of the interferometer. Diffraction order beams which carry the exact information of the thin film surface, are focused onto the pinhole with the first lens (60 mm focal length). This pinhole has two apertures on it. Zero-order component, which is passed through the 200 μm aperture of the pinhole, is a reference beam while first-order beam (+1) is a sample beam filtered from the 4 mm aperture. These two beams are interfered with each other at the camera plane by the second lens (150 mm focal length). In this experiment, Hamamatsu Orca Flash 4.0 camera was used. The total magnification of the system, calculated by multiplication of objective and the interferometer magnification, is 100. At last, the reference and the sample surface interferograms are saved to the computer. CdS thin film surface interferogram is indicated in Fig. 5. Surface profiles of the thin film are calculated by FT, CWT with Morlet, Pau, GMW and ST from these interferograms and are shown in Fig. 6. The phase values for the line x = 150 are compared in Fig. 7.

For imaging of CdS thin film surface, DPM has the advantage of being non-invasive, high accuracy, and speed. The thin film surface profile has been obtained in the radian unit and a deposit on the surface and surface roughness have been observed (Fig. 6). Fig. 7 shows that the results retrieved by ST are close to each other with the Morlet wavelet. FT has given a different and rough solution than all. It can be seen that the phase values calculated by Paul wavelet and GMW are more sensitive than the others.
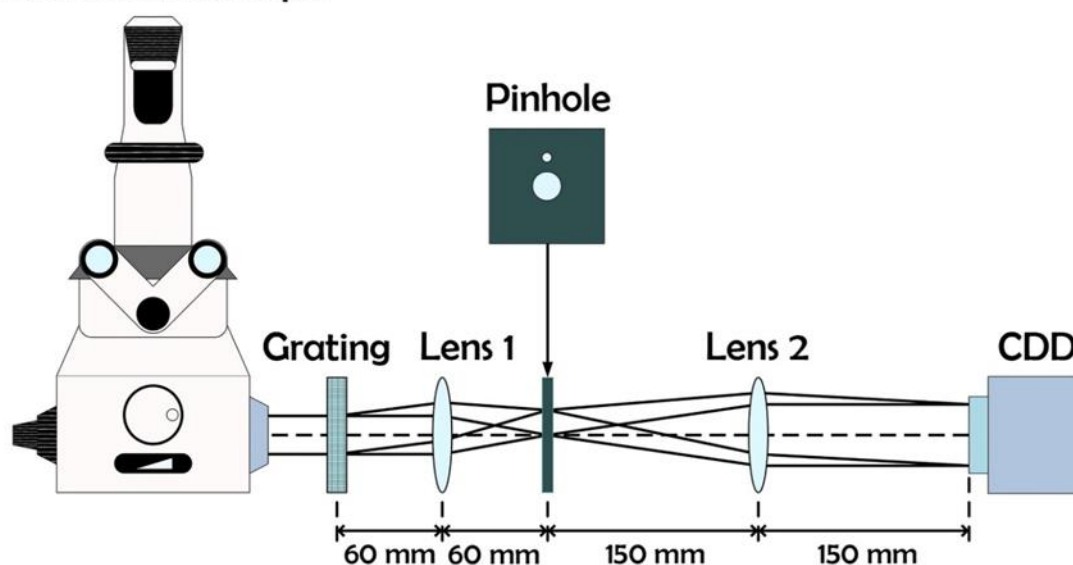
Fig. 4 White light DPM setup with a Mach–Zehnder interferometer and an optical microscope.
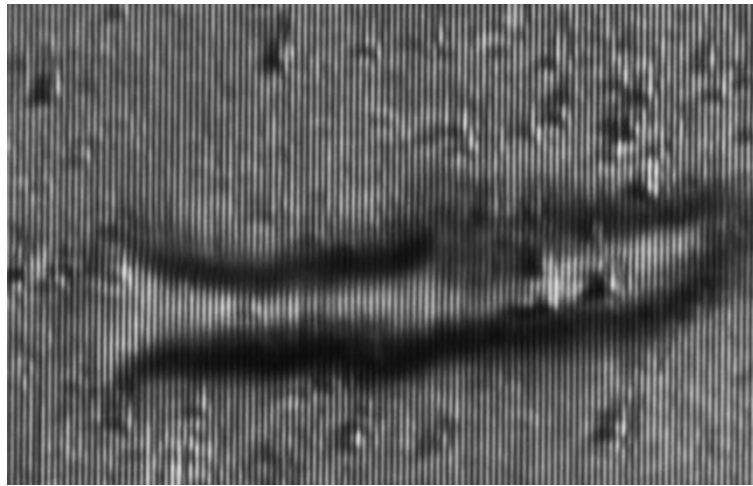
Fig. 5 The CdS thin film surface interferogram.
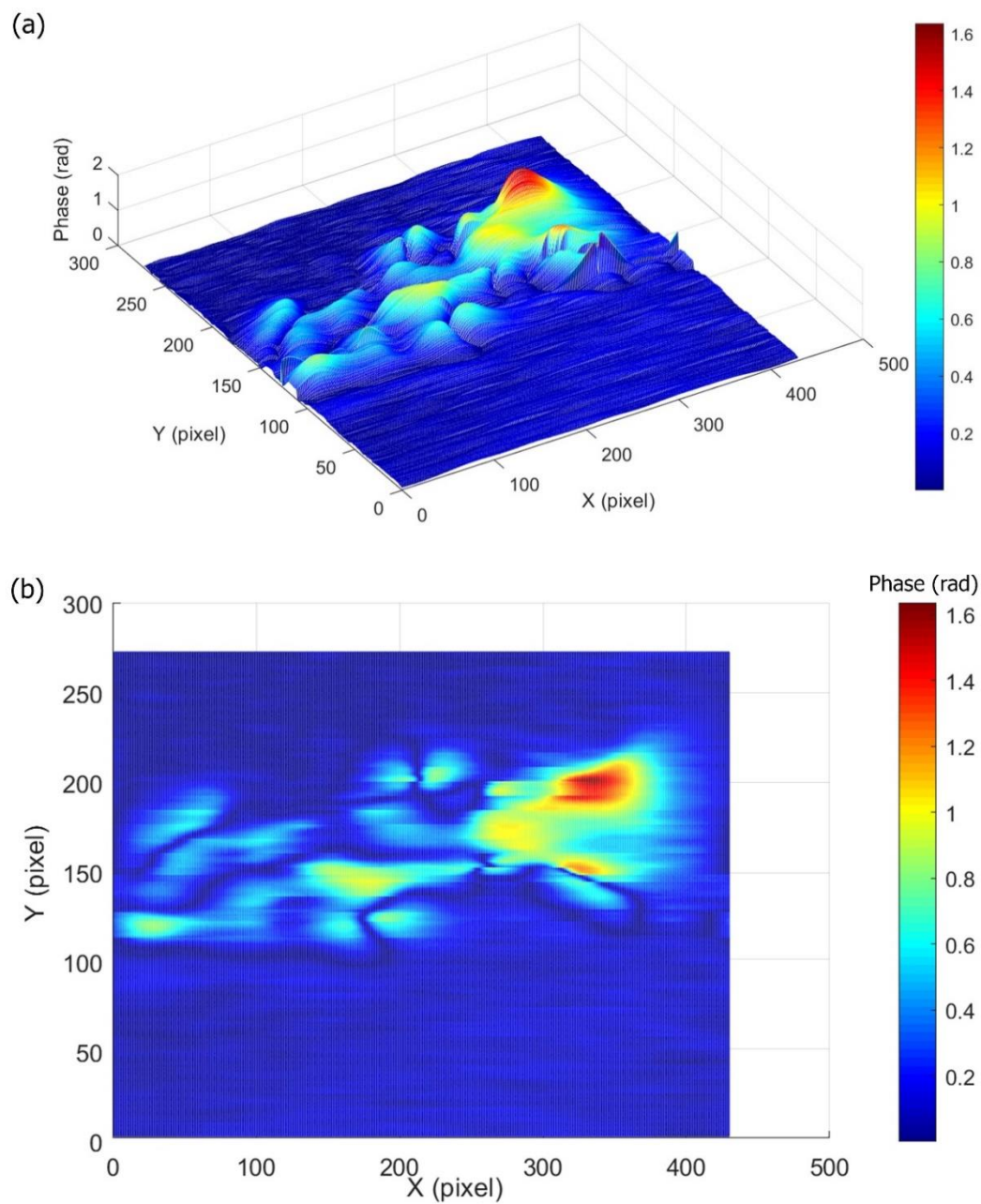
Fig. 6 (a) The recovered 3D phase profile of the thin film surface by CWT phase method with GMW (β=10; γ=3); (b) front view.
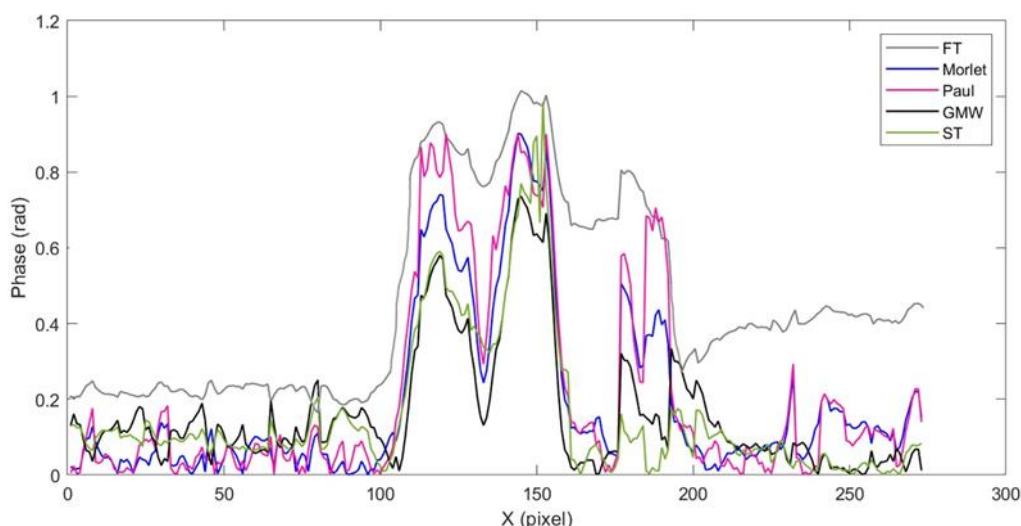
Fig. 7 The phase values for the line x = 150 by FT, CWT with Morlet, Paul (n=10), GMW (β=10; γ=3) and ST.

6. Conclusion

The phase calculation methods have been compared in terms of precision and implementation. FT and CWT have commonly used methods of phase demodulation from an interferogram. ST is defined as a phase-corrected version of the CWT, which includes a Gaussian window. The Gaussian window has the translation parameter b, while the exponential kernel expression does not contain the b parameter. The exponential kernel non-shift allows independent localization of the real and imaginary parts of the spectrum while the window function is shifted in the x-space. [34]. The ST holds absolute referenced phase information, which is the phase information given by the ST referring to the sinusoid's argument at x=0. This has the same meaning of phase as given by the FT. CWT is capable of finding the local power spectrum. The basic philosophy of the CWT is that the mother wavelet can decompose the signal with a scale and translation parameters. The phase of the CWT is calculated according to the centre of the wavelet. Thus, as the wavelet translates, the reference point of the phase translates and the resulting phase is defined as the locally referred phase [35], [43], [44]. Therefore, both the wavelet and the reference point of the phase are translated. The retrieved phase this way is defined as the locally referenced phase. FT and CWT are not related to each other in terms of the role of the phase. This is the reason why the phase result obtained from the CWT method is different from the Fourier transform method. The ST method establishes a relationship between frequency-dependent resolution and the absolutely referenced phase [35]. Unlike CWT, ST estimates both the local power spectrum and the local phase spectrum at the same time. This difference in the implementation of the ST method allows for the determination of the phase without reconstructing the image and thus phase information is found with less error [36].

The simulation and experimental results are attractive in that DPM is very convenient for thin film surface measurement and an extra degree of freedom leads to controling the precision of the measurement.

Declaration

Author Contribution: Conceive-O.K.; Design-O.K.; Supervision-O.K.; Experimental Performance, Data Collection and/or Processing-O.K., E.T.; Analysis and/or Interpretation-O.K., E.T; Literature Review-O.K.; Writer-O.K.; Critical Reviews –O.K., E.T.

Conflict of Interest: There are not any conflicts of interest for all authors.

ORCID ID

Özlem KOCAHAN https://orcid.org/0000-0002-6168-7147
Erhan TIRYAKI https://orcid.org/0000-0002-9791-3206

References

[1] G. Popescu, Y. K. Park, W. Choi, R. R. Dasari, M. S. Feld, and K. Badizadegan, "Imaging red blood cell dynamics by quantitative phase microscopy," *Blood Cells, Molecules, and Diseases*, vol. 41, no. 1, pp. 10–16, 2008, doi: 10.1016/j.bcmd.2008.01.010.

[2] X. Su and W. Chen, "Fourier transform profilometry:," *Optics and Lasers in Engineering*, vol. 35, no. 5, pp. 263–284, May 2001, doi: 10.1016/S0143-8166(01)00023-9.

[3] V. Dubey, G. Singh, V. Singh, A. Ahmad, and D. S. Mehta, "Multispectral quantitative phase imaging of human red blood cells using inexpensive narrowband multicolor LEDs," *Applied Optics*, vol. 55, no. 10, p. 2521, 2016, doi: 10.1364/ao.55.002521.

[4] A. Doblas, E. Sánchez-Ortiga, M. Martínez-Corral, G. Saavedra, and J. Garcia-Sucerquia, "Accurate single-shot quantitative phase imaging of biological specimens with telecentric digital holographic microscopy," *Journal of Biomedical Optics*, vol. 19, no. 4, p. 46022, 2014, doi: 10.1117/1.JBO.19.4.046022.

[5] M. Mir, B. Bhaduri, R. Wang, R. Zhu, and G. Popescu, "Quantitative Phase Imaging," in *Progress in Optics*, vol. 57, Elsevier Inc., 2012, pp. 133–217. doi: 10.1016/B978-0-44-459422-8.00003-5.

[6] H. Kwon, E. Arbabi, S. M. Kamali, M. S. Faraji-Dana, and A. Faraon, "Single-shot quantitative phase gradient microscopy using a system of multifunctional metasurfaces," *Nature Photonics*, vol. 14, no. 2, pp. 109–114, 2020, doi: 10.1038/s41566-019-0536-x.

[7] B. Bhaduri *et al.*, "Diffraction phase microscopy: principles and applications in materials and life sciences," *Advances in Optics and Photonics*, vol. 6, no. 1, p. 57, Mar. 2014, doi: 10.1364/AOP.6.000057.

[8] J. Nadeau, Y. K. Park, and G. Popescu, "Methods in quantitative phase imaging in life science," *Methods*, vol. 136, pp. 1–3, 2018, doi: 10.1016/j.ymeth.2018.03.004.

[9] B. Bhaduri, H. Pham, M. Mir, and G. Popescu, "Diffraction phase microscopy with white light," *Optics Letters*, vol. 37, no. 6, p. 1094, Mar. 2012, doi: 10.1364/OL.37.001094.

[10] G. Popescu, *Quantitative Phase Imaging of Cells and Tissues*. The McGraw-Hill Companies, Inc., 2011.

[11] K. Lee *et al.*, "Quantitative Phase Imaging Techniques for the Study of Cell Pathophysiology: From Principles to Applications," *Sensors*, vol. 13, no. 4, pp. 4170–4191, Mar. 2013, doi: 10.3390/s130404170.

[12] I. Moon, F. Yi, Y. H. Lee, B. Javidi, D. Boss, and P. Marquet, "Automated quantitative analysis of 3D morphology and mean corpuscular hemoglobin in human red blood cells stored in different periods," *Optics Express*, vol. 21, no. 25, p. 30947, 2013, doi: 10.1364/oe.21.030947.

[13] S. Wang, K. Yan, and L. Xue, "Quantitative interferometric microscopy with two dimensional Hilbert transform based phase retrieval method," *Optics Communications*, vol. 383, no. October 2016, pp. 537–544, Jan. 2017, doi: 10.1016/j.optcom.2016.10.008.

[14] G. Popescu, T. Ikeda, R. R. Dasari, and M. S. Feld, "Diffraction phase microscopy for quantifying cell structure and dynamics," *Optics Letters*, vol. 31, no. 6, p. 775, 2006, doi: 10.1364/OL.31.000775.

[15] H. Majeed *et al.*, "Magnified Image Spatial Spectrum (MISS) microscopy for nanometer and millisecond scale label-free imaging," *arXiv*, vol. 26, no. 5, pp. 6731–6736, 2018, doi: 10.1364/oe.26.005423.

[16] M. Takeda and K. Mutoh, "Fourier transform profilometry for the automatic measurement of 3-D object shapes," *Applied Optics*, vol. 22, no. 24, p. 3977, Dec. 1983, doi: 10.1364/ao.22.003977.

[17] S. Ma, C. Quan, R. Zhu, C. J. Tay, L. Chen, and Z. Gao, "Micro-profile measurement based on windowed Fourier transform in white-light scanning interferometry," *Optics Communications*, vol. 284, no. 10–11, pp. 2488–2493, May 2011, doi: 10.1016/j.optcom.2011.01.041.

[18] S. Van der Jeught and J. J. J. Dirckx, "Real-time structured light profilometry: A review," *Optics and Lasers in Engineering*, vol. 87, pp. 18–31, 2015, doi: 10.1016/j.optlaseng.2016.01.011.

[19] Su, W. Chen, Q. Zhang, and Y. Chao, "Dynamic 3-D shape measurement method based on FTP," *Optics and Lasers in Engineering*, vol. 36, no. 1, pp. 49–64, Jul. 2001, doi: 10.1016/S0143-8166(01)00028-8.

[20] W. Gao and Q. Kemao, "Statistical analysis for windowed Fourier ridge algorithm in fringe pattern analysis," *Applied Optics*, vol. 51, no. 3, p. 328, Jan. 2012, doi: 10.1364/AO.51.000328.

[21] R. Polikar, "THE WAVELET TUTORIAL," *2006 Index to Series of Tutorials to Wavelet Transform*, 2006.

[22] E. Coşkun, K. Sel, S. Özder, and M. Kurt, "Refractive index and extinction coefficient determination of an absorbing thin film by using the continuous wavelet transform method," *Applied Optics*, vol. 47, no. 27, p. 4888, Sep. 2008, doi: 10.1364/AO.47.004888.

[23] O. Kocahan, E. Tiryaki, E. Coskun, and S. Ozder, "Determination of phase from the ridge of CWT using generalized Morse wavelet," *Measurement Science and Technology*, vol. 29, no. 3, 2018, doi: 10.1088/1361-6501/aa9d56.

[24] A. Dursun, S. Özder, and F. N. Ecevit, "Continuous wavelet transform analysis of projected fringe patterns," *Measurement Science and Technology*, vol. 15, no. 9, pp. 1768–1772, Sep. 2004, doi: 10.1088/0957-0233/15/9/013.

[25] R. Watkins, "Review of fringe pattern phase recovery using the 1-D and 2-D continuous wavelet transforms," *Optics and Lasers in Engineering*, vol. 50, no. 8, pp. 1015–1022, 2012, doi: 10.1016/j.optlaseng.2012.01.001.

[26] C. Torrence and G. P. Compo, "A Practical Guide to Wavelet Analysis," *Bulletin of the American Meteorological Society*, vol. 79, no. 1, pp. 61–78, Jan. 1998, doi: 10.1175/1520-0477(1998)079<0061:APGTWA>2.0.CO;2.

[27] E. Coskun, S. Ozder, and E. Tiryaki, "The Paul wavelet algorithm: an alternative approach to calculate the refractive index dispersion of a dielectric film from transmittance spectrum," *Applied Physics B*, vol. 113, no. 2, pp. 243–250, May 2013, doi: 10.1007/s00340-013-5465-7.

[28] J. M. Lilly and S. C. Olhede, "Generalized Morse Wavelets as a superfamily of analytic wavelets," *IEEE Transactions on Signal Processing*, vol. 60, no. 11, pp. 6036–6041, Nov. 2012, doi: 10.1109/TSP.2012.2210890.

[29] J. M. Lilly and S. C. Olhede, "Higher-Order properties of analytic wavelets," *IEEE Transactions on Signal Processing*, vol. 57, no. 1, pp. 146–160, Jan. 2009, doi: 10.1109/TSP.2008.2007607.

[30] M. Zhong, F. Chen, C. Xiao, and Y. Wei, "3D surface profilometry based on 2D S-Transform method with optimized window," *Optik - International Journal for Light and Electron Optics*, vol. 139, pp. 87–94, 2017, doi: 10.1016/j.ijleo.2017.03.087.

[31] Q. Shen, W. Chen, M. Zhong, and X. Su, "An improving fringe analysis method based on the accuracy of S-transform profilometry," *Optics Communications*, vol. 322, pp. 8–15, Jul. 2014, doi: 10.1016/j.optcom.2014.01.056.

[32] R. G. Stockwell, L. Mansinha, and R. P. Lowe, "Localization of the complex spectrum: the S transform," *IEEE Transactions on Signal Processing*, vol. 44, no. 4, pp. 998–1001, Apr. 1996, doi: 10.1109/78.492555.

[33] S. Özder, Ö. Kocahan, E. Coşkun, and H. Göktaş, "Optical phase distribution evaluation by using an S-transform," *Optics Letters*, vol. 32, no. 6, p. 591, Mar. 2007, doi: 10.1364/OL.32.000591.

[34] R. G. Stockwell, "S -Transform Analysis of Gravity Wave Activity from a Small Scale Network of Airglow Imagers by," 1999.

[35] R. G. Stockwell, "A basis for efficient representation of the S-transform," *Digital Signal Processing*, vol. 17, no. 1, pp. 371–393, Jan. 2007, doi: 10.1016/j.dsp.2006.04.006.

[36] Y. Wang, "Efficient Stockwell Transform with Applications to Image Processing by," 2011.

[37] X. Su and W. Chen, "Fourier transform profilometry: a review," vol. 35, pp. 263–284, 2001.

[38] Z. Zhang, Z. Jing, Z. Wang, and D. Kuang, "Comparison of Fourier transform, windowed Fourier transform, and wavelet transform methods for phase calculation at discontinuities in fringe projection profilometry," *Optics and Lasers in Engineering*, vol. 50, no. 8, pp. 1152–1160, Aug. 2012, doi: 10.1016/j.optlaseng.2012.03.004.

[39] I. Daubechies and T. Paul, "Time-frequency localisation operators-a geometric phase space approach: II. The use of dilations," *Inverse Problems*, vol. 4, no. 3, pp. 661–680, Aug. 1988, doi: 10.1088/0266-5611/4/3/009.

[40] M. Afifi, A. Fassi-Fihri, M. Marjane, K. Nassim, M. Sidki, and S. Rachafi, "Paul wavelet-based algorithm for optical phase distribution evaluation," *Optics Communications*, vol. 211, no. 1–6, pp. 47–51, Oct. 2002, doi: 10.1016/S0030-4018(02)01828-X.

[41] S. C. Olhede and A. T. Walden, "Generalized Morse Wavelets," *IEEE Transactions on Signal Processing*, vol. 50, no. 11, pp. 2661–2670, Nov. 2002, doi: 10.1109/TSP.2002.804066.

[42] Ö. Kocahan, E. Coşkun, and S. Özder, "Generalized Morse wavelets for the phase evaluation of projected fringe pattern," *Measurement Science and Technology*, vol. 25, no. 10, p. 105701, Oct. 2014, doi: 10.1088/0957-0233/25/10/105701.

[43] E. Coskun, "İnce Filmlerin Optik Özelliklerinin İntegral Dönüşüm Yöntemleri ile Belirlenmesi," 2012.

[44] L. R. Watkins, S. M. Tan, and T. H. Barnes, "Determination of interferometer phase distributions by use of wavelets," *Optics Letters*, vol. 24, no. 13, p. 905, Jul. 1999, doi: 10.1364/OL.24.000905.

[45] A. Ünal, Ö. Kocahan, B. Altunan, A. Aksoy Gündoğdu, M. Uyanık, and S. Özder, "Quantitative phase imaging of erythrocyte in epilepsy patients," *Microscopy Research and Technique*, no. December, pp. 1–9, 2020, doi: 10.1002/jemt.23676.